Monolayer iron oxide film on platinum promotes low temperature CO oxidation

Y.-N. Sun, Z.-H. Qin, M. Lewandowski, E. Carrasco, M. Sterrer, S. Shaikhutdinov *, H.-J. Freund

Abteilung Chemische Physik, Fritz-Haber-Institut der Max-Plank-Gesellschaft, Faradayweg 4-6, Berlin 14195, Germany

ARTICLE INFO

ABSTRACT

CO oxidation on a clean Pt(1 1 1) single crystal and thin iron oxide films grown on Pt(1 1 1) was studied at different $CO:O_2$ ratios (between 1:5 and 5:1) and partial pressures up to 60 mbar at 400–450 K. Structural characterization of the model catalysts was performed by scanning tunnelling microscopy, low energy electron diffraction, Auger electron spectroscopy and temperature-programmed desorption. It was found that monolayer FeO(1 1 1) films grown on Pt(1 1 1) were much more active than clean Pt(1 1 1) and nm-thick Fe_3O_4(1 1 1) films at all reaction conditions studied. Post-characterization of the catalysts revealed that at $CO:O_2 > 1$ the FeO(1 1 1) film dewets the Pt surface with time, ultimately resulting in highly dispersed iron oxide particles on Pt(1 1 1). The film dewetting was monitored *in situ* by polarization-modulated infrared reflection absorption spectroscopy. The reaction rate at 450 K exhibited first order for O_2 and non-monotonously depended on CO pressure. In O_2-rich ambient the films were enriched with oxygen while maintaining the long-range ordering. Based on the structure-reactivity relationships observed for the FeO/Pt films, we propose that the reaction proceeds through the formation of a well-ordered, oxygen-rich FeO_x ($1 < x < 2$) film that reacts with CO through the redox mechanism. The reaction-induced dewetting in fact deactivates the catalyst. The results may aid in our deeper understanding of reactivity of metal particles encapsulated by thin oxide films as a result of strong metal–support interaction.

© 2009 Elsevier Inc. All rights reserved.

1. Introduction

The nature of an oxide support plays an important role in catalytic reactions over highly dispersed noble metal catalysts. At a given particle size, the support effects are often rationalized in terms of reactions taking place at the metal/oxide interface or involving spillover of reactive species onto/from an oxide support. These mechanisms are usually considered for transition metal oxides such as titania and ceria. On the other hand, metals supported on the reducible oxides often exhibit the so-called strong metal-support interaction (SMSI) [1–6], which in many cases manifests itself by encapsulation (decoration) of the metal particles by a thin layer stemming from the oxide support. Formation of thin titania layers on Pt and Pd particles upon heating *in vacuo* has recently been investigated by high-resolution scanning tunnelling microscopy (STM) [7–9]. It is rather obvious that the decoration will suppress catalytic reactions occurring on metal surfaces and be particularly detrimental for structure sensitive reactions. On the other hand, the reversal of the SMSI state has been observed after CO hydrogenation reactions on Pt/TiO$_2$ [10,11]. Also, partial recovering of CO uptake (as a test for the metal encapsulation) upon oxidative treat-

ments of Pt/TiO$_2$(1 1 0) and Pt/CeO$_2$(1 1 1) model catalysts has been reported [12,13]. Reversible wetting–dewetting behaviour induced by ambient conditions has recently been demonstrated by *in situ* STM on vanadia overlayer on Pd(1 1 1) [14]. Therefore, reaction conditions may affect the surface structure and hence the reactivity of catalysts that underwent the encapsulation during catalyst's preparation.

We have recently shown that Pt supported on iron oxide Fe$_3$O$_4$(1 1 1) films also exhibits an SMSI effect via encapsulation which is driven by the high adhesion energies between Pt and iron oxide [15,16]. In particular, top facets of the Pt particles heated above 800 K in vacuum revealed the structure that is very similar to an ultrathin FeO(1 1 1) film grown on a Pt(1 1 1) single crystal [17]. This finding suggests that the FeO(1 1 1)/Pt(1 1 1) film is a suitable model system for studying the behaviour of the encapsulated Pt particles.

The adsorption properties of FeO(1 1 1) as well as of Fe$_3$O$_4$(1 1 1) and Fe$_2$O$_3$(0 0 0 1) films under ultrahigh vacuum conditions were reviewed by Weiss and Ranke [18]. Under the conditions typically used in temperature-programmed desorption/reaction (TPD, TPR) studies, the FeO films were essentially inert towards molecular adsorption (carbon monoxide, water, ethylbenzene and styrene). Therefore, the adsorption studies were primarily focused on surfaces of magnetite (Fe$_3$O$_4$) and hematite (Fe$_2$O$_3$) (see also [19,20]). The inertness of the FeO(1 1 1) film is believed to be

* Corresponding author. Fax: +49 30 8413 4105.
E-mail address: shaikhutdinov@fhi-berlin.mpg.de (S. Shaikhutdinov).

related to the fact that the surface exposes a close-packed layer of oxygen (the monolayer film stacks as O–Fe–Pt–Pt...). However, it is not obvious *per se* that the film will maintain the structure upon exposure to realistic reaction conditions. It has been demonstrated that adsorbates, molecules, metal atoms and clusters on thin oxide films supported on metallic substrates may, under certain conditions, induce electron transfer through the film onto the adsorbate [21–27]. Therefore, it is conceivable, that under favourable conditions such electron transfer in turn induces reactivity between molecules. Formation of an appropriate transition state with high probability is almost certainly enhanced under high-pressure conditions. If the chemical potential, set by the gas pressure, is such that one of the reacting components is oxygen, prone to exchange with the oxygen in the film, then restructuring of the film, accompanied by unexpected reactivity, could be observed.

In attempts to shed light on the possible effects of elevated pressures and temperatures on structure and reactivity of thin oxide films, we have recently initiated "high-pressure" studies of FeO/Pt films with respect to CO oxidation. To combine both, reactivity studies at atmospheric pressure and a structural control of model catalysts, we used a so-called "high-pressure" cell located inside an ultra-high vacuum (UHV) chamber equipped with different surface-science tools. The sample, having been prepared and characterized under UHV conditions, is sealed in the cell used as a reactor that allows using gas chromatography (GC) analysis of products. In particular, we have found that the FeO films in 40 mbar of CO + 20 mbar O_2 at 450 K show much higher CO_2 production than the clean Pt(1 1 1) surface [28]. Tentatively, this unexpected result has been explained on the basis of reaction-induced dewetting of the oxide film, resulting in highly dispersed FeO_x nanoparticles on Pt(1 1 1), thus effectively forming "inverted" catalysts [29].

In this paper, we report an extended study of the structure and reactivity of FeO films with respect to CO oxidation at different $CO:O_2$ ratios, partial pressures and reaction temperatures. The results suggest that the unusual activity of the ultra-thin FeO films is intimately connected to the formation of an oxygen-rich oxide film reacting with CO at steady state through a red-ox process. However, under CO-rich conditions, a dewetting of the film occurs that causes the catalyst's deactivation.

The paper is organized as follows. First, we show results on CO oxidation and structural characterization of the FeO films at stoichiometric $CO:O_2$ ratios. Then, we provide data on reactivity at different CO and O_2 ratios and partial pressures. Finally, we speculate on a general mechanism for the CO oxidation reaction on ultrathin FeO films.

2. Experimental

The experiments were performed in three UHV chambers ("TPD-GC", "STM" and "PM-IRAS"), equipped with low-energy electron diffraction (LEED), Auger electron spectroscopy (AES) and a quadrupole mass spectrometer (QMS). The TPD-GC chamber houses a high-pressure cell (~30 ml, made of Au-plated Cu massive block) connected to gas handling lines and a gas chromatograph GC 6890N (Agilent). The double-side polished Pt(1 1 1) crystal (~10 mm in diameter, 1.5 mm in thickness) was spot-welded to two parallel Ta wires, which were in turn welded to two Ta sticks used for resistive heating and also for cooling by filling a manipulator rod with liquid nitrogen. The temperature was measured by a chromel–alumel thermocouple spot-welded to the edge of the crystal and controlled using a feedback system (Schlichting Phys. Instrum.). The manipulator rod inside the chamber ends with a KF-type flange with a 4-pins electrical feedthrough holding Ta and thermocouple sticks. The reactor is sealed from the UHV chamber using a Viton O-ring placed on top of the reactor matching the flange on the rod.

For high-pressure experiments, CO (99.995%, Linde) and O_2 (99.999%, AGA GmbH) were additionally cleaned using a cold trap kept at ~200 K. The reaction mixtures of CO and O_2 were balanced by He to 1 bar in a gas handling system. After introduction to the high-pressure cell, the gas was circulating with a flow of 3 ml/min for 20 min at room temperature to equilibrate the reaction gas flow. During this pretreatment, no CO_2 formation was observed. Then the sample was heated up to the reaction temperature with a heating rate of 1 K/s. The gas composition in the circulating flow was analyzed using a HP-Plot Q column at 35 °C and a TCD detector. For structural characterization of the spent catalysts, the crystal was rapidly (within 2–3 min) cooled down to room temperature, and the reactor was pumped out down to ~10^{-5} mbar (which typically takes ~20 min) before exposing to UHV.

Basically, a similar design was used in the PM-IRAS chamber, where a single-side polished Pt(1 1 1) crystal was spot-welded by Ta wires to Mo rods on the manipulator for resistive heating. The temperature was controlled by a chromel–alumel thermocouple spot-welded to the backside of the crystal. After surface preparation and characterization, the sample was transferred into a stainless steel high-pressure cell (~1 l) sealed with differentially pumped, spring loaded Teflon O-rings. The cell was equipped with two CaF_2 windows for infrared reflection absorption spectroscopy (IRAS) studies using a Bruker IFS 66v spectrometer. Polarization modulated (PM) IRAS measurements were carried out with a wire-grid polarizer and a photoelastic modulator (Hinds Instruments PEM 90) which modulates the polarization of the incident infrared light between p- and s-polarized at a frequency of 74 kHz. In p-polarization, both surface and gas-phase species contribute to the absorption signal, while in s-polarization, only gas-phase species are detected. By calculating the differential absorbance $\Delta R/R = (R_p - R_s)/(R_p + R_s)$, where indexes s and p are referred to s- and p-polarizations, respectively, a vibrational spectrum of the surface species can be obtained.

In the STM chamber, the Pt(1 1 1) crystal was mounted to a Pt sample holder. The temperature was controlled using a chromel–alumel thermocouple spot-welded to the edge of the crystal. The crystal can be heated in the UHV chamber by electron bombardment from the backside using a tungsten filament. For treatments at high pressures the sample was transferred into the Au-plated reactor housing a heating stage, consisting of ceramic and sapphire pieces. The sample was heated from the backside using a halogen lamp. The STM images presented here were obtained at tunnelling currents of 0.5–0.8 nA and positive sample bias of 0.2–1 V.

The preparation of the ultra-thin FeO(1 1 1) and nm-thick Fe_3O_4(1 1 1) films on Pt(1 1 1) is described elsewhere [18]. Briefly, one monolayer (ML) of Fe (99.95%, Goodfellow) is deposited onto clean Pt(1 1 1) at 300 K and subsequently annealed in 10^{-6} mbar O_2 at 1000 K for 2 min. Repeated cycles of 5 ML Fe deposition and oxidation results in well-ordered Fe_3O_4(1 1 1) films.

3. Results and discussion

Before discussing reactivity of model catalysts at elevated pressures, it is instructive here to briefly summarize the results obtained by TPD and TPR for the adsorption and co-adsorption of CO and O_2 under UHV conditions.

The clean Pt(1 1 1) surface exposed to saturating amounts of O_2 (typically, 20 Langmuirs (L), 1 L = 10^{-6} Torr s) and subsequently CO at 100 K showed a broad CO_2 desorption signal centred at 315 K. In the opposite sequence or exposing the sample to the stoichiometric mixtures of CO and O_2 (2:1) at 100 K, no CO_2 was ob-

served in the TPR spectra. These results are consistent with the CO poisoning, a well-established effect on oxygen dissociation.

On the FeO(111)/Pt(111) surfaces, the individual TPD spectra of CO and O_2 inversely scale with the FeO coverage, with no difference in the temperature profiles as compared to the clean Pt(111), thus indicating no specific adsorption at the rim of FeO(111) islands formed at sub-monolayer coverage. As expected, the FeO(111) films fully covering Pt(111) do not show CO_2 formation in TPR spectra, since neither CO nor O_2 adsorbs on the O-terminated FeO(111) surface at the temperatures used. Note also that long exposures of the FeO films to 10^{-6} mbar CO at 500 K did not reveal any signature of oxide reduction. The results basically confirm the previous conclusions [18] about good thermal stability and chemical inertness of the FeO(111) films. However, the situation changes dramatically in the mbar-pressure range.

3.1. Structure and reactivity at stoichiometric $CO:O_2$ ratios

Fig. 1 shows CO_2 evolution upon slow heating of FeO(111) films in the mixture of 40 mbar CO and 20 mbar O_2 balanced by He to atmospheric pressure. Carbon dioxide is clearly observed at temperatures above 430 K. The reaction rate apparently increases at increasing temperature as shown in Fig. 2a presenting the kinetics of the CO_2 formation at different temperatures. At all temperatures studied, the oxidation rate decreases in time.

For comparison, the clean Pt(111) surface showed almost no activity under the same conditions (see Fig. 2b), that is consistent with the above-mentioned TPR results on CO self-poisoning. On the other hand, the well-ordered, nm-thick Fe_3O_4(111) films grown on Pt(111) also exhibited much lower activity than the FeO films, although higher than that of Pt(111). Therefore, the enhanced activity observed in these experiments must be intimately connected to the *ultrathin* FeO(111) film on Pt(111).

Furthermore, Fig. 2b shows that the reactivity of the FeO films strongly depends on the pressure while keeping the same $CO:O_2$ ratio. The reaction proceeds much slower when the pressure is reduced from 60 to 15 mbar, and then to 6 mbar. The latter fact points either to different reaction orders for CO and O_2 or pressure-dependent surface transformations, or both. Therefore, we first performed a structural characterization of the model catalysts after reaction.

Fig. 3 shows LEED patterns of the FeO/Pt surface as prepared (a) and after reaction in 60 mbar of a stoichiometric CO + O_2 mixture at 400 (b) and 450 K (c). The six-spots ring around integer spots is characteristic for the Moire superstructure that arises from the
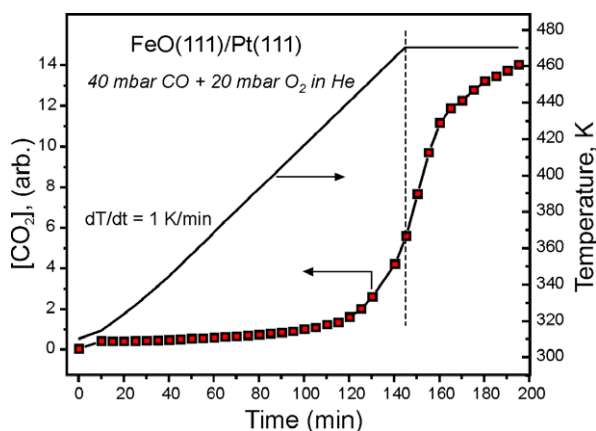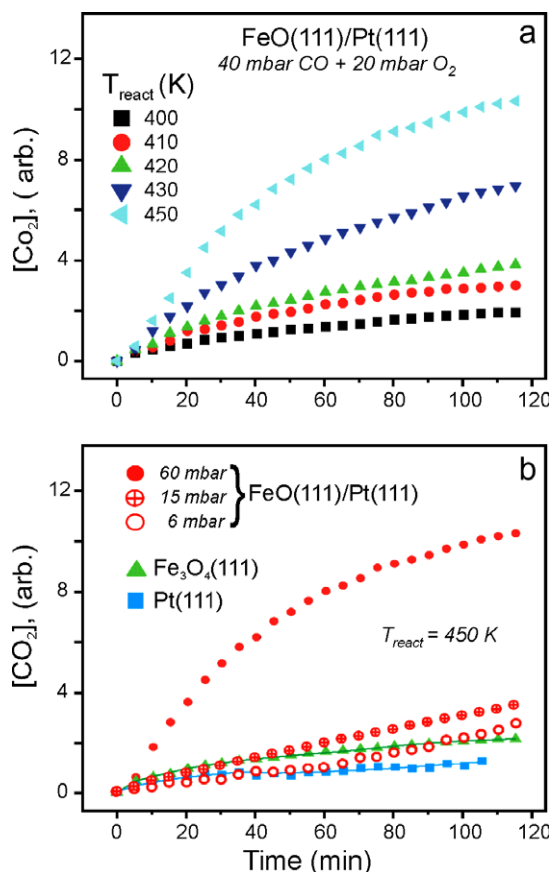

Fig. 2. Kinetics of CO_2 production over FeO(111)/Pt(111) in: (a) 40 mbar CO + 20 mbar O_2 at indicated temperatures; (b) at stoichiometric $CO:O_2$ (2:1) ratios at indicated total pressures at 450 K. The results for Pt(111) and nm-thick Fe_3O_4(111)/Pt(111) film in 40 mbar CO + 20 mbar O_2 at 450 K are shown in (b), for comparison. Time zero corresponds to the start of the sample heating (1 K/s) from 300 K.

mismatch between FeO(111) and Pt(111) lattices [17,18]. No changes are observed by LEED after the reaction at 400 K indicating that the surface preserves long-range ordering. The conclusion holds true also for the samples treated in 6 mbar at 450 K (not shown). On the contrary, the sample reacted at 450 K in 60 mbar of CO + O_2 showed the sharp diffraction spots of Pt(111) with additional weak spots (Fig. 3c), which are practically identical to those observed on clean Pt(111) by exposure to CO and assigned to a Pt(111)–c(4 × 2)CO structure [30]. At intermediate temperatures (∼430 K), a superposition of the FeO(111)/Pt(111) and CO/Pt(111) structures was observed. Therefore, we conclude that the FeO(111) films undergo strong reconstruction resulting in a surface exposing a significant fraction of Pt(111).

The AES study of the spent catalysts revealed only small amounts of carbon beyond the elements, which belong to the original surfaces, as shown in Fig. 4. (In particular, no nickel via Ni carbonyls which may contaminate CO in high-pressure containers has been detected.) Carbon (but no oxygen) has been found on the post-reacted Pt(111) surface most likely due to CO dissociation on the Pt low coordination sites [31]. Therefore, it seems plausible that carbon on the FeO/Pt surface appears in course of surface reconstructions whereby CO dissociates on the open Pt(111) areas. In addition, using the Auger O:Fe signal ratio in the pristine FeO films as a reference, the iron oxide phase in the post-reacted catalysts exhibits a $FeO_x(x \sim 1.25)$ stoichiometry, on average. Subsequent UHV annealing at temperatures above 800 K essentially restores both the LEED pattern and the O:Fe ratio of the original

Fig. 1. Temperature-programmed reaction profile of CO_2 production over FeO(111)/Pt(111) on slow heating (1 K/min) in 40 mbar CO + 20 mbar O_2 balanced by He.
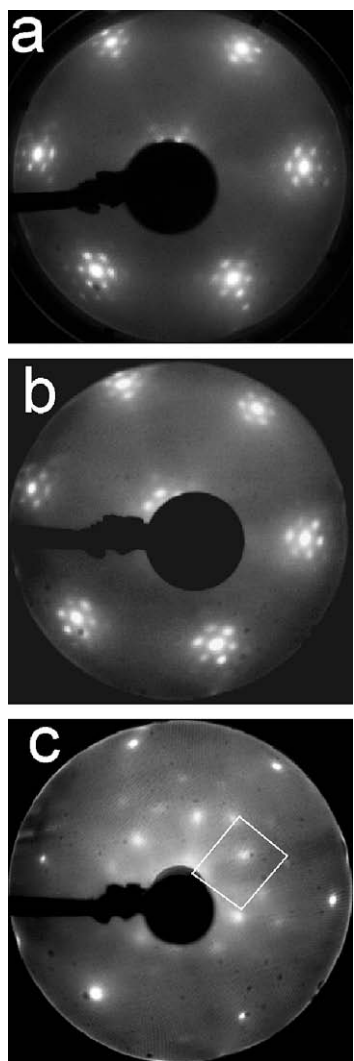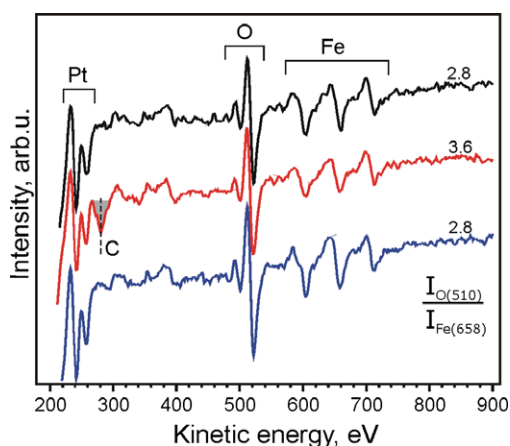
Fig. 3. LEED patterns of the "as prepared" FeO(1 1 1)/Pt(1 1 1) film (a) and after reaction at 400 (b) and 450 K (c) in 40 mbar CO + 20 mbar O_2 in He. The unit cell for c(4 × 2)CO–Pt(1 1 1) structure is indicated.

Fig. 4. AES spectra of the clean FeO(1 1 1)/Pt(1 1 1) film (top), after the reaction in 40 mbar CO + 20 mbar O_2 at 450 K (middle) and subsequent annealing to 800 K for 2 min (bottom). The corresponding peak ratios for O(510 eV) and Fe(658 eV) are indicated.

film and also removes carbon from the surface (see bottom spectrum in Fig. 4).

In line with LEED data, Auger spectra revealed no significant differences in the surface composition after catalytic tests at lower temperatures and/or lower pressures. The threshold temperature observed for the structural changes (∼430 K) basically coincides with the "ignition" temperature in the reaction profile shown in Fig. 1.

To determine the surface morphology of the model catalysts we employed STM. The Pt(1 1 1) surface after reaction essentially showed the original topography. Only few small, irregularly shaped particles, presumably of carbon (as judged by AES), and primarily located at the terrace steps were observed [28]. Fig. 5a shows an STM image of a FeO(1 1 1)/Pt(1 1 1) film with atomically flat, wide terraces exhibiting Moiré superstructure with a periodicity ∼2.6 nm. After 10 min exposure to the 40 mbar CO + 20 mbar O_2 mixture at 450 K, small particles emerge on the surface (see Fig. 5b), whereas the rest of the surface shows FeO-like superstructure. The large-scale STM images show that the reconstruction proceeds homogeneously on the whole film. After 120 min the surface is covered by nanoparticles as shown in Figs. 5c and 6a. The particles exhibit a narrow size distribution of 8 ± 1 nm in diameter and 1.8 ± 0.1 nm in height, and are assigned to iron oxide particles formed on Pt(1 1 1) upon dewetting of a FeO film. Stepwise annealing in UHV results in the oxide re-wetting (see Fig. 6), in full agreement with the LEED and AES results.

In order to obtain *in situ* information on surface restructuring we employed PM-IRAS that allowed monitoring surface species simultaneously with the gas-phase composition. Fig. 7a shows a series of spectra in the CO stretching region obtained from the FeO(1 1 1)/Pt(1 1 1) surface at 450 K in a reaction mixture of 40 mbar CO and 20 mbar O_2 (balanced by He). The spectrum for a Pt(1 1 1) crystal under the same conditions for 120 min is also shown for comparison.

The absorption band at ∼2095 cm^{-1} that grows with time is characteristic for atop (or terminal) CO species on Pt(1 1 1). In addition, a broad band centred at ∼1865 cm^{-1} develops, which is typical for CO occupying bridge position, i.e., consistent with the formation of c(4 × 2)-CO overlayer on Pt(1 1 1) observed by LEED. The integral intensity of two bands apparently saturates after ∼60 min of the reaction as shown in Fig. 7b, finally exposing approximately 70% of Pt(1 1 1). Therefore, the PM-IRAS results unambiguously show that an FeO film dewets a Pt substrate under the reaction conditions, thus exposing a Pt(1 1 1) substrate. Interestingly, the major peak at 2095 cm^{-1} revealed a low-frequency shoulder (centred at ∼2075 cm^{-1}), which remained after sample cooling and pumping the reactor out. Therefore, this feature can hardly be assigned to CO adsorbed on Lewis (Fe^{2+}) sites on iron oxide particles as CO desorbs from iron oxide surfaces below room temperature [32]. On the other hand, this feature is missing in the spectra for Pt(1 1 1) under the same conditions. Therefore, its presence on the dewetted surface could be linked to the oxide/metal interface formed upon dewetting.

Fig. 7b shows the time evolution of integral amounts of CO adsorbed on the surface and of CO_2 produced in the reaction as obtained by the respective surface and gas-phase IR signals. The kinetics of the CO_2 production resembles that of the GC experiments presented in Fig. 2, both showing that the CO oxidation rate (the slope of the CO_2 production curve) decreases with time. It is clearly seen that the highest rate is observed at the beginning of the reaction where the surface is essentially non-dewetted (see more in the next section). With increasing degree of dewetting the reaction rate slows down and stays practically constant as the maximum dewetting is obtained. At this stage, the CO_2 formation rate is almost equal to that observed for a Pt(1 1 1) single crystal (not shown here). Note that, under the conditions studied, the CO conversion is very low (<1%); therefore we can neglect the changes in the gas composition during the reaction.
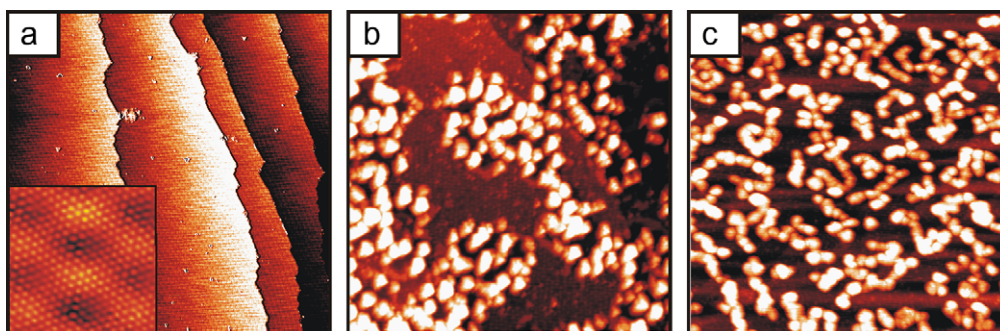
Fig. 5. STM images (size 200 nm × 200 nm) of the as prepared FeO(1 1 1) film (a), after 10 min (b) and 2 h (c) in 40 mbar CO + 20 mbar O_2 at 450 K. The inset shows the atomic structure of the Moire pattern.
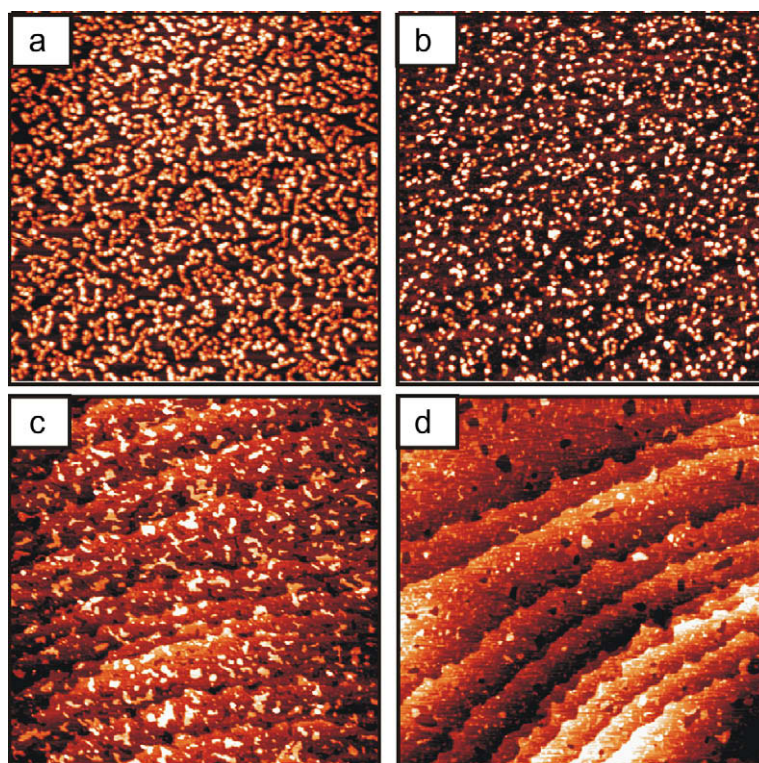
Fig. 6. STM images (size 500 nm × 500 nm) of the dewetted FeO(1 1 1) film (a) and after step-wise UHV annealing at 500 (b), 700 (c) and 800 K (d).

Further information on the structure of the post-reacted FeO/Pt surfaces was obtained by TPD. Only CO and CO_2 were found as desorbing species upon heating of the spent catalysts in UHV. After reaction at low temperatures, a broad and rather featureless CO desorption signal at 350–450 K is observed (Fig. 8). (Note that the pristine FeO films do not adsorb CO even at 90 K.) With increasing the reaction temperature, a peak at ∼390 K develops which superimposes with the signal at 320–500 K gaining intensity. Except the prominent feature at 380–390 K, the TPD spectra are similar to the one observed after CO adsorption on clean Pt(1 1 1) shown in the same graph for comparison. The desorption traces of CO and CO_2 at $T > 500$ K, which are missing in the spectra for Pt(1 1 1), may be attributed to the reaction of carbonaceous species with surface oxygen (e.g., see [39]). This oxygen is apparently coming from the iron oxide particles since the carbon peak in AES spectra disappears upon heating to 800 K with a simultaneous restoration of the Auger O:Fe ratio (see Fig. 6). Annealing at $T > 800$ K leads again to the chemical inertness towards CO, as it essentially recovers the structure of the FeO(1 1 1) films as judged by LEED, AES and STM.
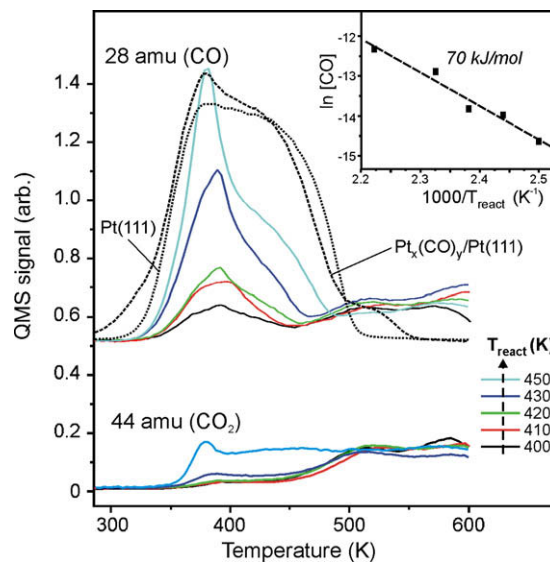
Regarding the desorption peak at ∼380 K, it cannot be assigned to CO adsorbed on iron oxide particles [32]. Note that this peak was only observed on strongly dewetted surfaces (e.g., after reaction in 60 mbar at 450 K) and never under O-rich reaction conditions (see below). Also, the peak does not show up in the next CO TPD runs, i.e., after the first heating to 600 K. On the other hand, narrow CO desorption signals are typical for decomposition of metal carbonyls (e.g., [33,34]). Indeed, $Pt_x(CO)_y$ species prepared on Pt(1 1 1) by physical vapour deposition of Pt in 10^{-6} mbar of CO at 100 K revealed a similar TPD peak at ∼380 K superimposed with the signal from CO/Pt(1 1 1) as shown in Fig. 8. Therefore, we may assign this desorption feature, observed on the spent catalysts, to Pt carbonyl-like species formed upon film dewetting the Pt surface. Its absence on the post-reacted Pt(1 1 1) sample indicates that these species are probably stabilized by the iron oxide particles formed. This conclusion is also consistent with the observation of a low-frequency shoulder on the 2095 cm^{-1} band on FeO/Pt and not on Pt(1 1 1) surface in the PM-IRAS experiments (see Fig. 7a).
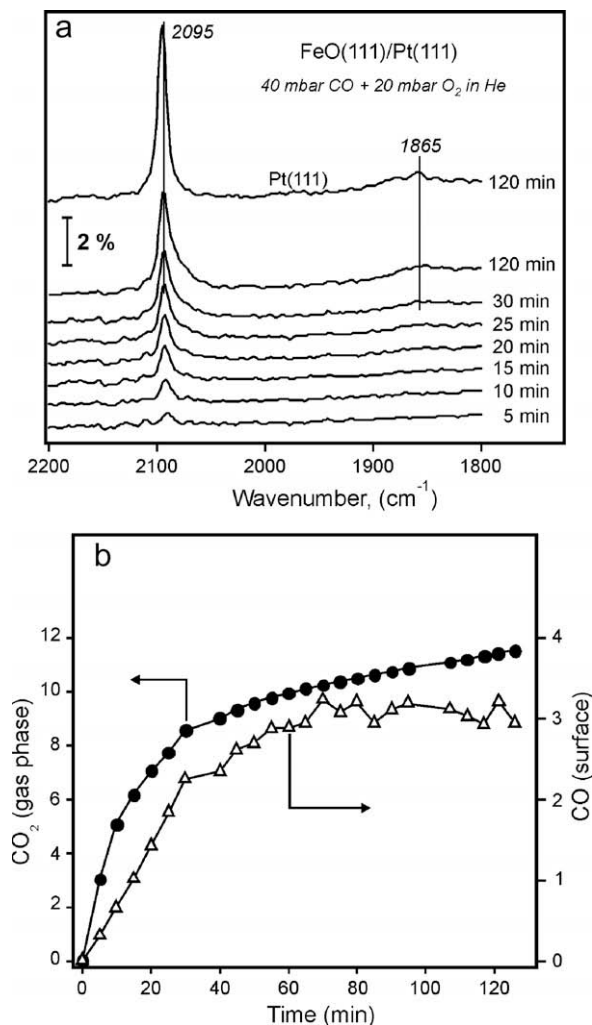
Fig. 7. (a) Time-resolved PM-IRAS spectra of the CO stretching region obtained from the FeO(1 1 1)/Pt(1 1 1) surface at 450 K in a mixture of 40 mbar CO and 20 mbar O_2 balanced by He to 1 bar. The spectrum for the Pt(1 1 1) surface after 120 min at the same conditions is shown for comparison. (b) Kinetics of CO_2 formation in the gas phase and of CO adsorbed on FeO(1 1 1)/Pt(1 1 1) obtained by integration of the respective PM-IRAS signals.

Fig. 8. CO (28 amu) and CO_2 (44 amu) signals in TPD spectra of a FeO(1 1 1)/Pt(1 1 1) film reacted in 40 mbar CO + 20 mbar O_2 for 120 min at indicated temperatures. The samples were cooled to 300 K and evacuated to 10^{-5} mbar before exposing to UHV. The inset shows the Arrhenius plot for the integral CO desorption signal as a function of reaction temperature. The spectrum for clean Pt(1 1 1) after reaction at 450 K is shown as dotted line for comparison. TPD spectrum of $Pt_x(CO)_y$ formed on Pt(1 1 1) by Pt deposition in 10^{-6} mbar of CO at 100 K (dashed line) is shown to highlight a desorption feature at ~380 K.

One could, in principle, suggest the formation of iron carbonyls upon reduction of the FeO film at high CO pressures. However, previous studies showed that $Fe_x(CO)_y$ species (x = 1–3; y = 5–12) exhibit the 2064 cm^{-1} band as the highest for the terminal CO stretch (e.g., [34–36]), which is well below than the shoulder at 2075 cm^{-1} observed in Fig. 7a. Formation of highly reduced or metallic Fe particles adsorbing CO can be excluded either. Indeed, CO on oxide supported Fe nanoparticles showed the band at ~2030 cm^{-1} [37]. In addition, if formed upon the reduction of the FeO film, the Fe overlayer on Pt(1 1 1) would manifest itself by the IRAS signal either at ~1950 cm^{-1} (at 343 K) or at 2060 cm^{-1} (at 473 K), the latter being due to Fe migration into the sub-surface region as reported in [38]. All scenarios are inconsistent with the spectra shown in Fig. 7a.

In addition to PM-IRAS, we used the TPD results for estimating the degree of dewetting (determined here as a percentage of the Pt(1 1 1) substrate that opens during a reaction) by integrating the CO TPD signal between 300 and 500 K. Using the TPD spectrum for CO/Pt(1 1 1) as a reference, we found that approximately 70% of the surface expose the Pt(1 1 1) after reaction at 450 K for 2 h. This value nicely agrees with that obtained by PM-IRAS. It has turned out that the integral CO intensity vs reaction temperature relation-

ship fits well the Arrhenius plot as shown in the inset in Fig. 8, from which the activation energy ~70 kJ/mol is calculated. The analysis with a proper subtraction of the feature at ~380 K in the TPD spectra results in a bit smaller value, ~65 kJ/mol. Therefore, 65–70 kJ/mol may be considered in the first approximation as the activation energy for the FeO film dewetting; however, this value will depend on pressure and CO:O_2 ratio.

Note that according to the TPD studies, no dewetting is observed after individual exposures of FeO films to 40 mbar CO or 20 mbar O_2 at 450 K. In both cases, the LEED patterns revealed a Moire superstructure. It is therefore clear that dewetting is a reaction-induced process.

3.2. O_2-rich vs CO-rich reaction conditions

It is well documented in the literature that the CO oxidation rate on Pt catalysts strongly depends on CO:O_2 partial pressures ([39,41] and references therein). Therefore, one may raise the question about whether the promoting effect of the ultrathin FeO films exists in a wide range of CO and O_2 partial pressures. To study possible effects of the gas composition on reactivity of the FeO films, we carried out two sets of experiments in various CO + O_2 mixtures. In the first set, we varied the O_2 pressure while keeping the CO partial pressure at 10 mbar. In the second one, we kept the O_2 partial pressure constant at 20 mbar and varied the CO pressure. In two sets the CO:O_2 ratio was varied between 1:5 and 5:1 which basically covers both O_2- and CO-rich regimes. The mixtures were always balanced by He to 1 bar, and the reaction was monitored at 450 K. After reactivity measurements, the surfaces were characterized by LEED, TPD and AES.

Fig. 9 shows the kinetics of CO_2 production at different CO and O_2 partial pressures. Under CO-lean conditions the reaction rate is almost constant in time and increases while approaching 100% conversion of CO. In contrast, the reaction slows down in the CO-rich conditions. Note that the reaction rate was not much affected by CO_2 accumulation in the circulating gas mixture. Pumping out
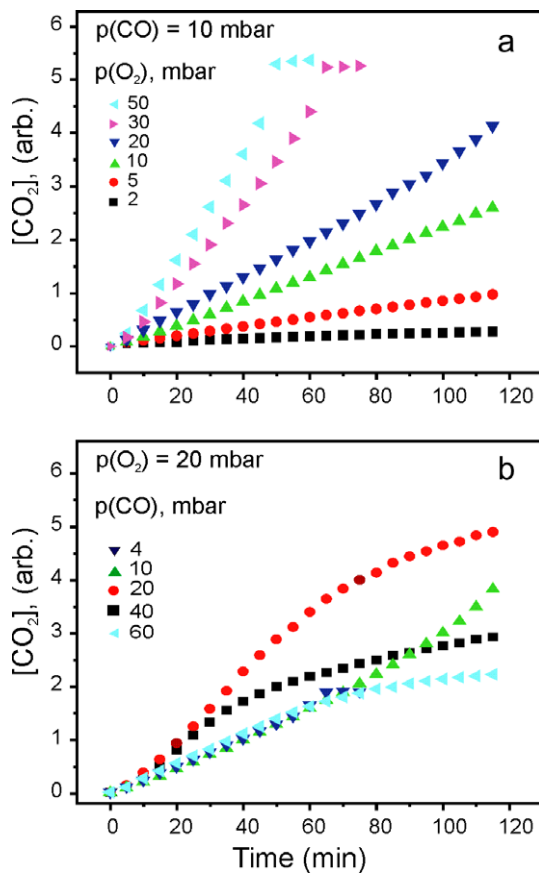
Fig. 9. Kinetics of CO_2 production at 450 K at different CO and O_2 partial pressures as indicated. Full conversion can be reached at low $CO:O_2$ ratios. Note the reaction rate slows down in CO-rich conditions ($CO:O_2 > 1$).

Fig. 10. Reaction rate (a), average stoichiometry (b) and degree of dewetting (c) of the spent FeO/Pt catalysts as a function of O_2 pressure in the mixture with 10 mbar of CO, balanced by He. Reaction temperature is 450 K.

the reactor and refilling the line with a fresh CO + O_2 mixture had basically no effect on the subsequent activity, thus indicating that CO_2 is not involved in the deactivation process. For further analysis we present the rates measured in the first minutes of reaction (i.e., extrapolated to zero conversion on yet non-deactivated catalysts), if not specified.

Fig. 10a depicts the reaction rate as a function of oxygen pressure. The reaction kinetics exhibits first order ($n = 1.1 \pm 0.1$) for O_2. This may straightforwardly explain the results of Fig. 2b showing much lower CO_2 production upon decreasing the total CO + O_2 (2:1) pressure from 60 down to 6 mbar. The reaction order measured on Pt(1 1 1) under the same conditions is close to unity ($n = 0.85 \pm 0.1$) and is consistent with the previous studies [42]. The figure shows that the FeO/Pt catalysts exhibit much higher activity than Pt(1 1 1) in the whole pressure range studied.

The temperature dependence of the reaction rate measured at 410–450 K in the mixture of 10 mbar CO and 20 mbar O_2 leads to an Arrhenius plot with an apparent activation energy of 113 ± 5 kJ/mol. Due to the very low conversion, it was impossible to precisely measure the activation energy on Pt(1 1 1) for comparison. Nevertheless, this value is significantly lower than ~135 kJ/mol, reported for supported Pt catalysts and Pt single crystal surfaces for conditions where CO is the primary surface species [40,42], which is in turn very close to the desorption energy of CO from Pt [30,31].

The reaction is accompanied by remarkable structural changes detected by AES. The film becomes enriched with oxygen upon increasing O_2 pressure, and approaches the O:Fe ratio close to 2, on average (see Fig. 10b). Interestingly, the corresponding LEED
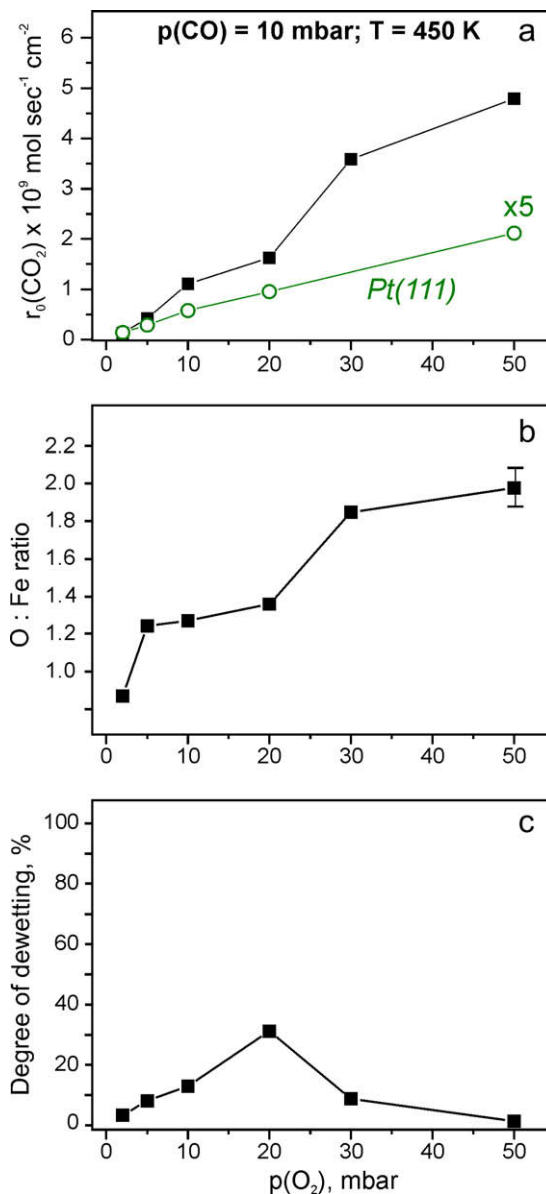
patterns (not shown here) are in fact similar to those of the pristine FeO(1 1 1)/Pt(1 1 1) surface. Another intriguing finding is that the degree of dewetting (see Fig. 10c) basically shows no direct relationship to activity (Fig. 10a). In fact, in the O_2-rich atmosphere the inverse relation is observed such that the activity is the highest for the least dewetted surface.

In the next step, we review experimental results of the second set of experiments. Fig. 11 shows the reaction rate (a), average stoichiometry of the iron oxide film (b) and degree of dewetting (c) as a function of CO partial pressure. Note that under the same conditions the Pt(1 1 1) surface showed zero-order kinetics for CO at 450 K, i.e., in full agreement with the previous studies [42]. Fig. 11a reveals again, that the FeO films are much more active than Pt(1 1 1) in the whole CO pressure range studied. The initial reaction rate vs CO pressure relationship is not monotonous and has a maximum at $CO:O_2 \sim 1$. Apparently, at high CO pressures the reaction exhibits negative reaction order, and the catalytic activity decreases with time (see Fig. 9b and also Fig. 2). The data
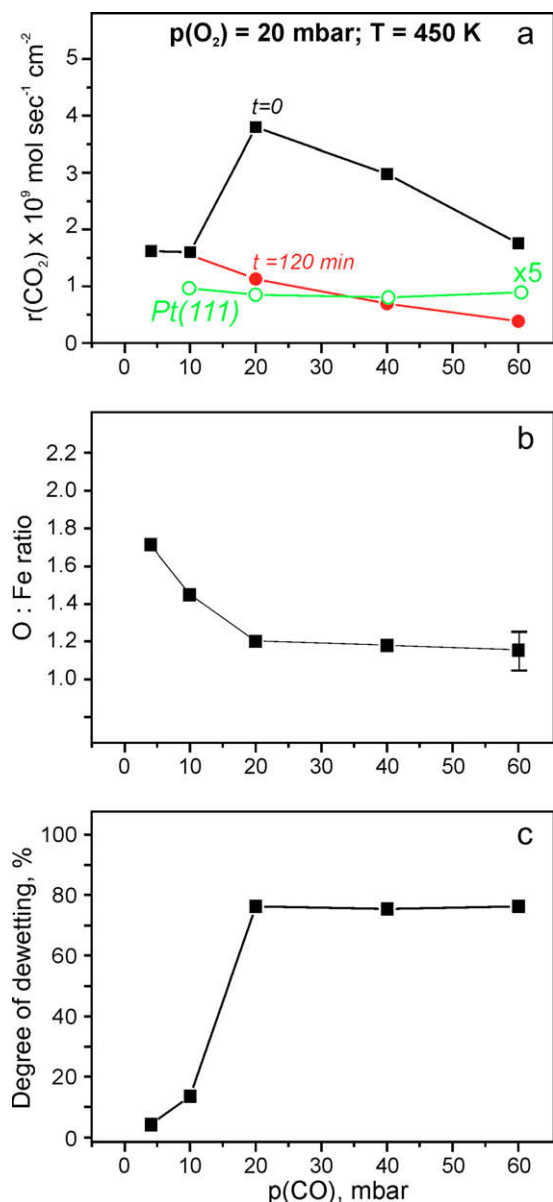
Fig. 11. Reaction rate (a), average stoichiometry (b) and degree of dewetting (c) of the spent FeO/Pt catalysts as a function of CO pressure in the mixture with 20 mbar of O_2, balanced by He. The reaction rates measured after 120 min on stream as well as data for clean Pt(1 1 1) are also shown.

measured after 2 h on stream are also shown in Fig. 10a, for comparison.

The dewetting process remarkably accelerates at CO pressures above 10 mbar (see Fig. 11c) leading to a degree of dewetting of ∼70 % as the upper limit. However, LEED and TPD inspections of selected samples after 20–30 min on stream, i.e., before the deactivation sets in, showed negligible dewetting. Note also that in the first set of experiments the highest activity is observed for the non-dewetted surfaces. Finally, the PM-IRAS results (see Fig. 7b) showed *in situ* that the reaction rate is the highest in the first minutes of reaction. Therefore, we conclude that dewetting in fact causes the catalyst's deactivation rather than forming the most active phase as originally proposed [28].

Finally, under O-rich conditions, the iron oxide becomes enriched with oxygen. Interestingly, O-enrichment apparently mirrors the degree of dewetting (see Fig. 11b and c).

3.3. General discussion and proposed mechanism

The key observations presented in the previous sections can be summarized as follows.

(i) FeO(1 1 1) monolayer films grown on Pt(1 1 1) show much higher CO oxidation activity than Pt(1 1 1) at 400–450 K in a wide range of CO:O_2 ratios (between 1:5 and 5:1). The effect is observed only in the mbar pressure range.

(ii) The reaction is accompanied by strong structural transformations. In O_2-rich ambient, the films become enriched with oxygen while maintaining the long-range ordering. Under CO-rich conditions, the films undergo dewetting that causes the catalyst's deactivation. Dewetting is a reaction-induced process and cannot be observed in pure O_2 or CO ambient.

(iii) The reaction rate at 450 K exhibits first order for O_2 and non-monotonously depends on CO pressure.

In addition, it appears that the reaction does not exhibit an induction period, or the latter is shorter than our acquisition time (∼5 min) (see Figs. 2 and 9). Under O-rich conditions, the film is enriched with oxygen and does not undergo dewetting that in turn slows down the reaction rate in the CO-rich atmosphere (see Figs. 9–11). These findings suggest that the surface of the O-rich film formed at elevated O_2 partial pressures is in fact the most active. The surface transformations resulting in this surface seem to be relatively fast since the reaction rate in the O-rich atmosphere is practically constant from the onset.

The lack of structural information of the reconstructed FeO$_x$ film surface renders the reaction mechanism uncertain. Oxidation reactions on oxides are usually considered within a Mars–van Krevelen scheme [43] which invokes a surface redox process where the reactant is oxidized by lattice oxygen and the reduced catalyst is subsequently reoxidized by molecular oxygen. However, the recent analysis by Vannice [44] revealed a number of inconsistencies in the assumptions incorporated into the derivation of the rate expression, even though still the experimental data may be fitted.

Oxidation of CO on iron oxides (Fe_2O_3) has been previously studied both experimentally and theoretically [45–48]. The reaction is typically carried out at temperatures above 500 K in excess of oxygen, although the reaction may occur even in the absence of external oxygen over iron oxide nanoparticles [45]. It was found that the reaction proceeds through dissociative adsorption of O_2, which is considered to be a non-activated process, and removal of oxygen by a gas-phase CO via an Eley–Rideal type mechanism. The reaction showed zero-order kinetics for O_2 and first order for CO at 520–570 K [44,45]. Microkinetic modelling revealed that the reaction between CO and surface O species is the rate-determining step [46]. The Eley–Rideal mechanism was corroborated theoretically for the (1 0 0) surface of Fe_2O_3, whereas on the oxygen terminated (0 0 0 1) surface the preference towards the Langmuir–Hinshelwood mechanism (i.e., CO adsorption before reaction with O) was observed [47].

Certainly, in these studies the bulk structure of iron oxide was assumed to remain unchanged during reaction, whereas the monolayer FeO films undergo strong transformations, which should be taken into account in the reaction kinetics. Our results showed first-order kinetics for O_2, i.e., in variance to the above-mentioned iron oxides catalysts showing zero order. Therefore, it may well be that the oxygen pressure dependence reflects the kinetics of structural transformations resulting in the O-rich phase rather than the reaction itself. It seems plausible that the whole reaction starts with the formation of the O-rich surface domains, which react with CO producing CO_2. The lattice oxygen is then replenished from the gas phase. In excess of CO the formation of the O-rich film competes with the film reduction accompanied by dewetting.

The atomic structure of the O-rich surface is still unclear. However, we may speculate on possible structures. The FeO films, either treated by pure O_2 or reacted at low $CO:O_2$ ratios at 450 K, showed LEED patterns, which are very similar to those of the pristine FeO(111)/Pt(111) surface. On the other hand, these films accommodate much more oxygen (without loosing Fe), thus approaching the average Fe:O ratio close to 1:2 as judged by AES (see Fig. 10b). Therefore, we have tentatively proposed that a FeO film, originally composed of Fe and O close-packed layers stacked as O–Fe/Pt, reconstructs at high O_2 pressures into a O–Fe–O/Pt-like ("sandwich") structure. Indeed, STM images of the FeO(111) films treated with 20 mbar of O_2 at 450 K showed long-range modulation which is very similar to that of pristine FeO (Fig. 12).

Certainly, whenever reactions at elevated pressures are carried out, very careful attention needs to be considered towards impurities in the feedstock, particularly to those having high reaction probability. There are evidences in the literature showing that oxide surfaces may be very sensitive to the traces of water in an ambient, even in the vacuum background [49,50].

In order to see whether water and hydrogen as impurities in the reaction ambient affect the reactivity data presented in Figs. 9–11, we have performed experiments in the TPD-GC setup using the mixture of 10 mbar CO + 50 mbar O_2 with additional 0.5 mbar of water. The results showed no effect of water on reactivity under these conditions. Meanwhile, adding 0.5 mbar of H_2 to a CO + O_2 mixture dramatically increased the reaction rate, by factor of 2. However, in the latter case the FeO(111) film reconstructs in a different manner, and the reaction most likely proceeds through the different mechanism (to be discussed in forthcoming paper).

In addition, we have examined thermal stability of the O-rich FeO_x films formed by exposure to 20 mbar O_2 at 450 K for 20 min. The TPD spectra on heating to 1200 K (not shown) showed ~90% increase of oxygen content as compared to the pristine film, i.e. consistent with the AES results presented in Figs. 10 and 11, but did not reveal water desorption. Only tiny amounts of water, as calibrated by water TPD on pristine FeO [51], was found desorbing in a broad signal at 400–700 K upon adding 0.15 mbar of H_2 into 20 mbar of O_2. Therefore, the TPD results suggest no hydroxyls to be present on the O-rich film surface under reaction conditions.

On the other hand, IRAS study of the FeO films exposed to 20 mbar of O_2 at 300 K in the PM-IRAS setup, having much higher reactor volume (~1 l vs 30 ml in GC setup), revealed an absorption band at 3642 cm^{-1} that shifts to 3625 cm^{-1} upon heating to 450 K. This band corresponds to the stretching mode of "isolated" (not H-bonded) OH species. The band stayed basically unchanged after pumping oxygen out and disappeared upon heating in vacuum above 500 K, accompanied by water desorption clearly seen in TPD spectra. The unexpected observation of surface hydroxyls on the O_2-treated films can be explained either by impurities in the feedstock or those are formed by reactions on the stainless steel reactor walls and gas handling lines. These species were not observed in 10 mbar of pure CO and 1 mbar of pure H_2, and only with minor abundance in 1 mbar of water. Note that the latter amounts are far above those expected as impurity in the reactor filled with 20 mbar of O_2. These findings therefore suggest that OH species are in fact formed as a result of the reaction of H_2 or water with the film first formed upon interaction of FeO with O_2. It appears that O-rich film is extremely reactive towards traces of hydrogen (or water) in the background, ultimately forming OH species. The resulted film is probably reminiscent of iron oxyhydroxides. Whether this may be connected to results on reduction of FeO films with atomic hydrogen [52,53] is not clear yet.

4. Summary

In this paper, we have shown that a thin FeO film exhibits enhanced activity towards CO oxidation as compared to clean Pt(111) and the nm-thick Fe_3O_4(111) films in a wide range of $CO:O_2$ ratios at 450 K. Post-characterization of the model catalysts using STM, LEED, AES and TPD shows that the reaction most likely proceeds through the formation of an oxygen-rich FeO_x ($1 < x < 2$) film that reacts with CO via the redox mechanism. The O-rich film tends to dewet at $CO:O_2 > 1$, ultimately resulting in highly dispersed iron oxide particles on Pt(111). The film dewetting was monitored in situ by PM-IRAS. The wetting/dewetting process is reversible depending on the ambient conditions.
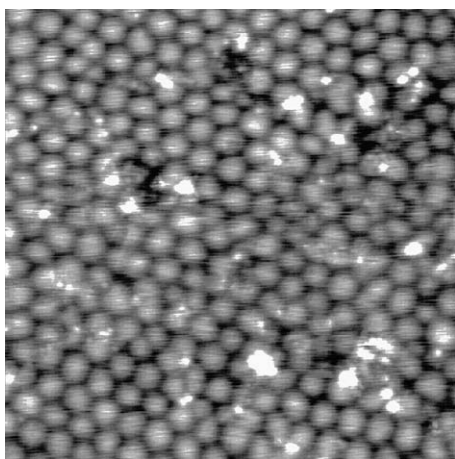
Such strong restructuring of the O-terminated FeO surface, in particular the formation of the well-ordered, oxygen-rich film at elevated O_2 pressures, implies an enhanced reactivity of ultrathin films towards gas phase molecules, otherwise inert at low pressures and/or on thick oxide films. This situation apparently links the reactivity of a thin oxide film to the presence of a metal substrate underneath and electron transfer processes recently highlighted in the literature [21–27]. In turn, the results may aid in our deeper understanding of the reactivity of metal particles encapsulated by oxide films as a result of strong metal-support interaction, e.g., Pt/TiO$_2$, Pt/CeO$_2$ and Pt/Fe$_3$O$_4$. Vibrational and electron spectroscopy studies with the goal to identify the nature of the oxygen rich phase are underway.

Fig. 12. STM image (50 nm × 50 nm) of the FeO film treated in 20 mbar of O_2 at 450 K for 10 min, showing that the film basically maintains long-range ordering (compare Fig. 5a).

References

[1] S.J. Tauster, S.C. Fung, R.L. Garten, J. Am. Chem. Soc. 100 (1978) 170.
[2] E. Ko, R. Garten, J. Catal. 68 (1981) 233.
[3] S.J. Tauster, Acc. Chem. Res. 20 (1987) 389.
[4] F. Solymosi, J. Catal. 94 (1985) 581.
[5] G.L. Haller, D.E. Resasco, Adv. Catal. 36 (1989) 173.
[6] F. Pesty, H.P. Steinrück, T.E. Madey, Surf. Sci. 339 (1995) 83.
[7] O. Dulub, W. Hebenstreit, U. Diebold, Phys. Rev. Lett. 84 (2000) 3646.
[8] M. Bowker, P. Stone, P. Morrall, R. Smith, R. Bennett, N. Perkins, R. Kvon, C. Pang, E. Fourre, M. Hall, J. Catal. 234 (2005) 172.
[9] F. Silly, M.R. Castell, J. Phys. Chem. B 109 (2005) 12316.
[10] K.J. Blankenburg, A.K. Datye, J. Catal. 128 (1991) 186.

[11] A.K. Datye, D.S. Kalakkad, M.H. Yao, D.J. Smith, J. Catal. 155 (1995) 148.
[12] S. Bernal, J.J. Calvino, M.A. Cauqui, J.M. Gatica, J.A. Perez Omil, J.M. Pintado, Catal. Today 50 (1999) 175.
[13] D.R. Mullins, K.Z. Zhang, Surf. Sci. 513 (2002) 163.
[14] S. Surnev, J. Schoiswohl, G. Kresse, M.G. Ramsey, F.P. Netzer, Phys. Rev. Lett. 89 (2002) 246101.
[15] Z.H. Qin, M. Lewandowski, Y.N. Sun, S. Shaikhutdinov, H.-J. Freund, J. Phys. Chem. C 112 (2008) 10209.
[16] Z.H. Qin, M. Lewandowski, Y.N. Sun, S. Shaikhutdinov, H.-J. Freund, J. Phys.: Condens. Matter 21 (2009) 134019.
[17] H.C. Galloway, P. Sautet, M. Salmeron, Phys. Rev. B 54 (1996) R11145.
[18] W. Weiss, W. Ranke, Prog. Surf. Sci. 70 (2002) 1.
[19] R.S. Cutting, C.A. Muryn, G. Thornton, D.J. Vaughan, Geochim. Cosmochim. Acta 79 (2006) 3593.
[20] K. Abib, D.R. Mullins, G. Totir, N. Camillione, J.P. Fitts, K.T. Rim, G.W. Flynn, R.M. Osgood, Surf. Sci. 537 (2003) 191.
[21] G. Pacchioni, L. Giordano, M. Baistrocchi, Phys. Rev. Lett. 94 (2005) 226104.
[22] H.-J. Freund, G. Pacchioni, Chem. Soc. Rev. 37 (2008) 2224.
[23] H.-J. Freund, Surf. Sci. 601 (2007) 1438.
[24] M. Sterrer, T. Risse, U.M. Pozzoni, L. Giordano, M. Heyde, H.P. Rust, G. Pacchioni, H.-J. Freund, Phys. Rev. Lett. 98 (2007) 096107.
[25] M. Sterrer, T. Risse, M. Heyde, H.-P. Rust, H.-J. Freund, Phys. Rev. Lett. 98 (2007) 206103.
[26] H. Grönbeck, J. Phys. Chem. B 110 (2006) 11977.
[27] P. Frondelius, A. Hellman, K. Honkala, H. Hakkinen, H. Grönbeck, Phys. Rev. B 78 (2008) 085426.
[28] Y.-N. Sun, Z.H. Qin, M. Lewandowski, S. Kaya, S. Shaikhutdinov, H.J. Freund, Catal. Lett. 126 (2008) 31.
[29] K. Hayek, M. Fuchs, B. Klötzer, W. Reichl, G. Rupprechter, Top. Catal. 13 (2000) 55.
[30] G. Ertl, M. Neumann, K.M. Streit, Surf. Sci. 64 (1977) 193.
[31] K. McCrea, J. Parker, P. Chen, G. Somorjai, Surf. Sci. 494 (2001) 238.
[32] C. Lemire, R. Meyer, V.E. Nenrich, S. Shaikhutdinov, H.-J. Freund, Surf. Sci. 572 (2004) 103.
[33] J. Libuda, A. Sandel, M. Bäumer, H.-J. Freund, Chem. Phys. Lett. 240 (1995) 429.
[34] S. Sato, Y. Ukisu, Surf. Sci. 283 (1993) 137.
[35] S. Fletcher, M. Poliakoff, J.J. Turner, Inorg. Chem. 25 (1986) 3597.
[36] R.L. Jackson, M.R. Trusheim, J. Am. Chem. Soc. 104 (1982) 6590.
[37] M.P. Felicissimo, O.N. Martyanov, T. Risse, H.-J. Freund, Surf. Sci. 601 (2007) 2105.
[38] T. Wadayama, H. Osano, T. Maeyama, H. Yoshida, K. Murakami, N. Todoroki, S. Oda, J. Phys. Chem. C 112 (2008) 8944.
[39] L. Schäfer, H.-W. Wassmuth, Surf. Sci. 208 (1989) 55.
[40] A.K. Santra, D.W. Goodman, Electrochim. Acta 47 (2002) 3595.
[41] R. Imbihl, G. Ertl, Chem. Rev. 95 (1995) 697.
[42] P.J. Berlowitz, C.H.F. Peden, D.W. Goodman, J. Phys. Chem. 90 (1988) 5213.
[43] P. Mars, D.W. van Krevelen, Chem. Eng. Sci. 38 (1954) 41.
[44] M.A. Vannice, Catal. Today 123 (2007) 18.
[45] P. Li, D.E. Miser, S. Rabiei, R.T. Yadav, M.R. Hajaligol, Appl. Catal. B 43 (2003) 151.
[46] S. Wagloehner, D. Reichert, D. Leon-Sorzano, P. Balle, B. Geiger, S. Kureti, J. Catal. 260 (2008) 305.
[47] A.K. Kandalam, B. Chatterjee, S.N. Khanna, B.K. Rao, P. Jena, B.V. Reddy, Surf. Sci. 601 (2007) 4873.
[48] H. Randall, R. Doepper, A. Renken, Ind. Eng. Chem. Res. 36 (1997) 2996.
[49] O. Bikondoa, C.L. Pang, R. Ithnin, C.A. Muryn, H. Onishi, G. Thornton, Nature Mater. 5 (2006) 189–192.
[50] R. Schaub, E. Wahlström, A. Rønnau, F. Besenbacher, Science 299 (2003) 377; R. Schaub, E. Wahlström, A. Rønnau, F. Besenbacher, Science 314 (2006) 925.
[51] J.L. Daschbach, Z. Dohnalek, S.-R. Liu, R.S. Smith, B.D. Kay, J. Phys. Chem. B 109 (2005) 10362.
[52] W. Huang, W. Ranke, Surf. Sci. 600 (2006) 793.
[53] L.R. Merte, J. Knudsen, L.C. Grabow, R.T. Vang, E. Lægsgaard, M. Mavrikakis, F. Besenbacher, Surf. Sci. 603 (2009) L15.